FIELD EVALUATION OF NDT DEVICES FOR DELAMINATION DETECTION OF HMA
AIRPORT PAVEMENTS

By:
Manuel Celaya
Advanced Infrastructure Design (AID)
1 Crossroads Drive, Hamilton, NJ, 08648
Phone: (609) 838-2216; Fax: (609) 586-1301
mcelaya@aidpe.com

and
Soheil Nazarian
Center for Transportation Infrastructure Systems (CTIS)
The University of Texas at El Paso (UTEP)
500 West University Av., El Paso, Texas 79968
Phone: (915)747 6925; Fax: (915)747 8037
nazarian@utep.edu

PRESENTED FOR THE
2014 FAA WORLDWIDE AIRPORT TECHNOLOGY TRANSFER CONFERENCE
Galloway, New Jersey, USA

August 2014

ABSTRACT

To ensure the desired structural capacity of flexible pavements, sufficient bonding between the hot mix asphalt (HMA) layers is essential. If lack of bonding is present, it may lead to delamination or debonding. This problem is particularly more severe on airfield pavements, due to higher traffic loads applied by aircrafts. Undetected delamination and associated cracks may result in stripping of the lower layers due to moisture intrusion or peeling away of thin lifts from the surface. Moreover, further progression of delamination may develop other dangerous distresses such as foreign object debris (FOD).

Rapid nondestructive test (NDT) methods to determine the presence and extent of delamination in asphalt pavements are highly desirable. Previous studies have investigated promising NDT procedures and equipment that have the potential to address the problem. The most promising NDT methods include Ground Penetrating Radar (GPR), seismic methods, mechanical impulse methods and thermography. These methods were previously evaluated on controlled pavement sections specifically constructed to simulate an airfield pavement. The theoretical and practical strength and limitations of these methods were identified and discussed as well.

Field evaluation of NDT technologies has not been extensively conducted. The focus of this paper is to present the results of these promising technologies at two major international airports in the US. The objective was to assess capabilities and practicality of selected NDT methods under actual field conditions. Results were also compared with cores retrieved at selected locations. Overall, Impulse Response and ultrasonic surface waves were the most successful methods, followed by the Falling Weight Deflectometer. The most effective methods are too slow and the rapid methods require improvements to their interpretation and analysis algorithms to be suitable for network level implementation.

INTRODUCTION

Structural adequacy and functionality of flexible pavements require proper interface bonding between adjacent asphalt layers. A poor bond and the subsequent delamination or debonding between layers reduces the serviceability and performance of a pavement. The lack of interface bonding may lead to several premature distresses including the most common types such as slippage, cracking, peeling and distortion. Moreover, if delamination goes undetected, it can ultimately result in the peeling away of thin lifts from the surface of the roadway (Road Management & Engineering Journal [1]).

Delamination typically occurs on areas of poor bond between the surface and binder courses, due to poor quality tack coat material or insufficient application. Moreover, areas experiencing high temperatures or high loads (especially horizontal loads) or a combination of the two are at greater risk. Airfield pavements are particularly more prone to delamination or debonding problems due to higher traffic loads applied by aircrafts. This situation is more critical on runways at the high-speed taxiway exits, where airplanes brake and turn (Bognacki et al. [2]), or at areas under large horizontal load of aircraft at takeoff, creating slippage due to inadequate bonding between the top layer and the layer below. Moreover, jet blasts from aircrafts can accentuate the problem by converting debonded fragments into foreign object debris (FOD).

Delamination and associated problems require frequent and expensive maintenance and may lead to a premature need for major rehabilitation. For those reasons, rapid detection of delamination with NDT devices, especially under field testing conditions is highly desirable. The focus of delamination detection should be on layers close to the surface (say the top 5 in.). The presence of a delaminated layer at any depth is undesirable, but under heavy traffic, delamination deeper than 8 in. poses small risk of surface distress (Hammons et al. [3]).

Previous studies evaluated the feasibility of estimating the presence and extent of HMA delamination with NDT methods under controlled conditions. Among those, Celaya et al. [4] narrowed down about a dozen technologies to four most feasible ones capable of locating debonded areas. These methods included Ground-coupled Ground Penetrating Radar (GPR), Impulse Response (IR), Ultrasonic Surface Waves (USW), and Falling Weight Deflectometer (FWD) and were extensively evaluated on a pavement section specifically constructed to address the needs of this study.

Furthermore, Celaya et al. [5] performed a comprehensive evaluation of these methods to provide an overall ranking of the methods. In that study, the technical and practical parameters that most likely affect the successful detection of debonding with NDT methods were considered. Those parameters included the accuracy, reproducibility, detectability threshold, speed of data collection, and the speed and sophistication of data analysis. Based on that ranking, the IR was ranked the highest, with the PSPA and FWD using the deflection of the first sensor (sensor under the load plate) ranking closely with it. The ground penetrating radar, which has the potential for rapid data collection, did not seem as feasible as the others.

Even though the evaluation of the methods under controlled condition is highly valuable, the unanticipated variability in the field conditions and the vastly different operational parameters on actual projects should also be considered. For that matter, the NDT methods and test protocols were evaluated on several features of two major US airports in this study. A brief literature review on the selected NDT methods for detection of delamination in HMA pavements is presented first. Typical results obtained with the different methods are described next. Validation results obtained with selected NDT methods at the two airports investigated and the summary and conclusions of this study are introduced.

## IDENTIFIED NDT METHODS FOR DETECTING DELAMINATION OF HMA

A detailed description and a comprehensive summary of the case histories of the utilization of about a dozen NDT methods for detecting debonding can be found in Celaya et al. [4]. For the sake of the brevity, only a brief introduction of the most feasible methods are provided in this paper.

Ground Penetrating Radar

GPR uses electromagnetic pulses to test, characterize, or detect changes in electromagnetic properties of the subsurface layers. The main advantage of the GPR is the speed of the operation and almost full-coverage of the pavement section. However, the application of GPR in detecting debonding has been mixed [6]. However, the latest developments in GPR technology using multi antenna arrays with frequency sweep have shown greater potential (Heitzman et al., [7]). The test setup used in this study is shown in Figure 1a. The equipment used consisted of a GSSI Model 5100 1.5 GHz ground-coupled antenna.
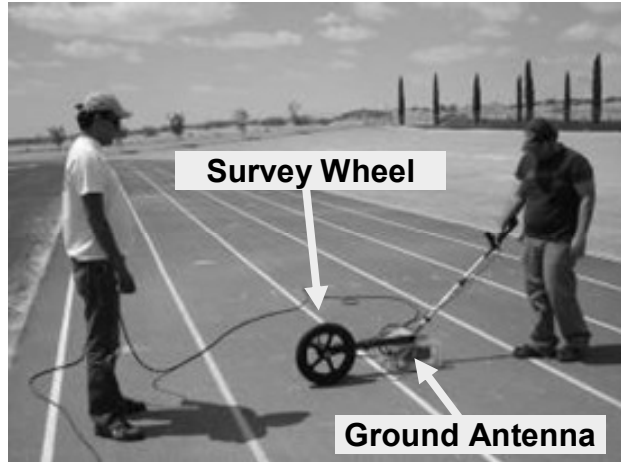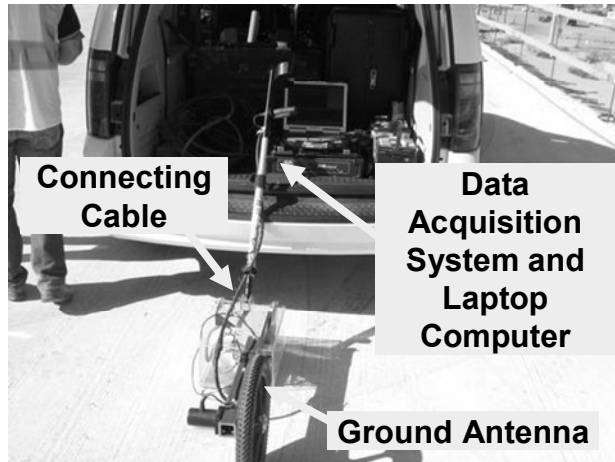
a) Ground Coupled GPR
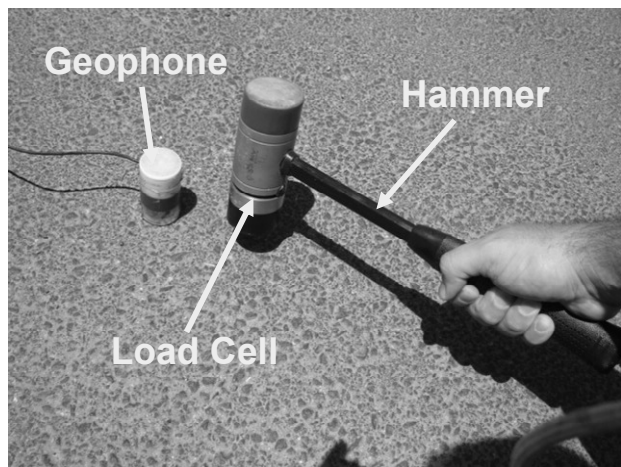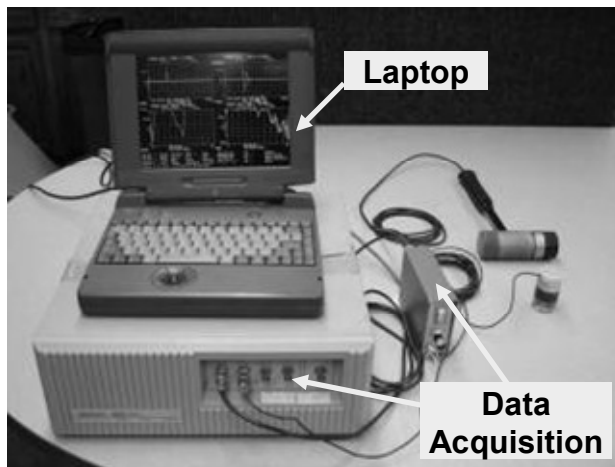
b) Impulse Response
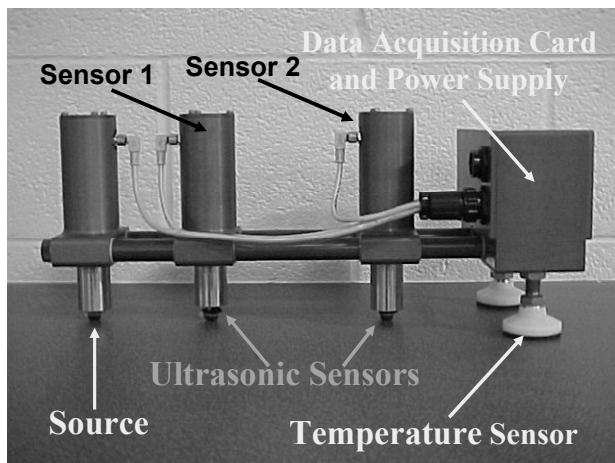
c) PSPA   d) FWD

Figure 1. Nondestructive Technologies Used in This Study.

Impulse Response Method

The basic operating principle of the IR method is to apply a short duration (<1 msec) impulse load to the pavement surface with an instrumented hammer and to measure the vertical displacement using a geophone. The short impulse duration would result in predominant vibration of the HMA layer. Kruntcheva et al. [8] successfully implemented this method for detection of debonding in controlled test sections. The equipment used in this study, as shown in Figure 1b, was a 10-lb hammer instrumented with a load cell and a 4.5-Hz geophone. Both the hammer and the receiver were connected to a portable field computer for data acquisition, storage and analysis.

Ultrasonic Surface Waves

The USW is a seismic-based method, in which the variation in surface wave velocity with wavelength is measured to generate a so-called dispersion curve. This method has been successfully used in detecting HMA stripping [3]. A Portable Seismic Property Analyzer (PSPA) was used in this study. The PSPA (see Figure 1c), consists of two ultrasonic transducers and a source packaged into a hand-portable system to conduct the USW tests (Nazarian et al., [9]). The outputs of the two transducers are subjected to signal processing and spectral analyses to estimate the variation in modulus with depth and an average modulus.

Falling Weight Deflectometer

Since the FWD (see Figure 1d) is well-known to the pavement community, it is not described here. The FWD readily provides the maximum load applied and up to nine maximum deflections, as well as the time histories of the load and deflections for more comprehensive analysis. In this study, a load of 9 kips and the deflections from seven sensors (equally spaced 12 in. apart) were used. After an extensive study, the most promising predictor of debonding with the FWD data was found to be either the deflection under the load plate normalized with maximum load or the backcalculated modulus of the HMA layer [4]. Conceptually, the FWD and IR tests seem very similar. However, since the pulse width of the load applied by FWD is about 60 msec (as opposed to less than 1 msec for IR), the base and subgrade (not the HMA) contribute to most of the measured deflections. Unlike the IR method, the influence of the non-uniformity in the thicknesses and moduli of the underlying layers brings about some uncertainty in the interpretation of the results for debonding (especially when they are not in advanced stages). Also the manifestation of HMA debonding is more pronounced in frequencies above 200 Hz, where the FWD impulse does not contain any energy.

TYPICAL RESULTS OBTAINED IN CONTROLLED STUDIES

As reported in Celaya et al., [5], ten different sections were constructed specifically for this study as depicted in Figure 2. Each section was 9 ft. long (2.7 m) by 10 ft. (3 m) wide. Three transition zones were incorporated to minimize the variability of the laid down mix during construction. The pavement cross-section for all sections consisted of a prepared sandy-silt subgrade and about 8 in. (200 mm) of HMA placed in three lifts. The bottom lift consisted of about 3 in. (75 mm) of a coarse (P-403) mix and the middle lift 2.5 in. (63 mm) of a fine (P-401) mix. The top lift (2.5 in. or 63 mm thick) of Sections 1 through 5 consisted of a coarse mix (P-403 mix) and Sections 6 through 10 a fine mix (P-401 mix).
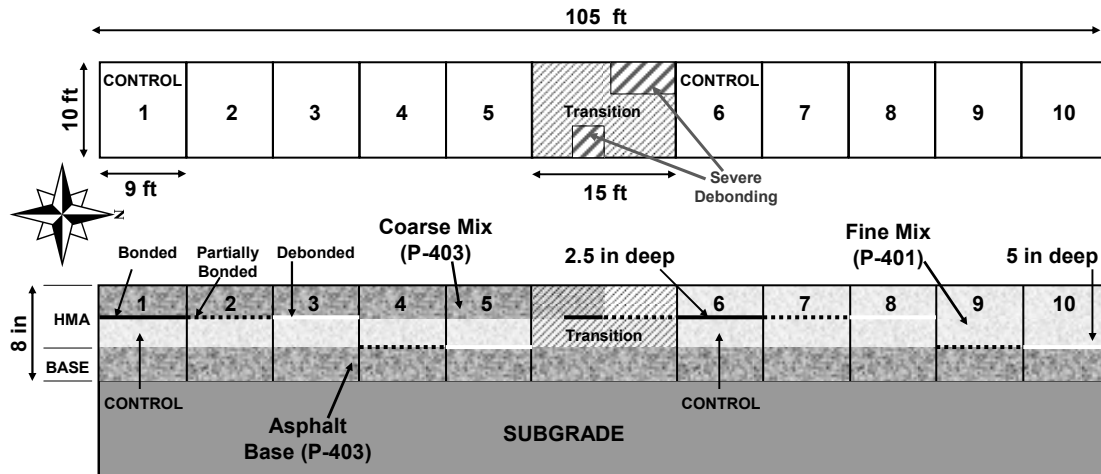
Figure 2. Schematic of Small Scale Section Constructed for this Study.

A typical plan view of each section and test locations are depicted in Figure 3. A 4 ft. (1.2 m) by 9 ft. (3 m) area for each section was intentionally debonded. In addition, smaller debonded areas were constructed to test the detectability threshold of the methods. A hundred points were investigated with each method on each section as indicated on Figure 3, except for the GPR that a continuous profile was obtained along each of the ten lines. The impact of temperature on the effectiveness of the test methods was evaluated by conducting tests in "cool" early spring temperatures (range of 60 to 85ºF) and "hot" summer temperatures (range of 75 to 120ºF).
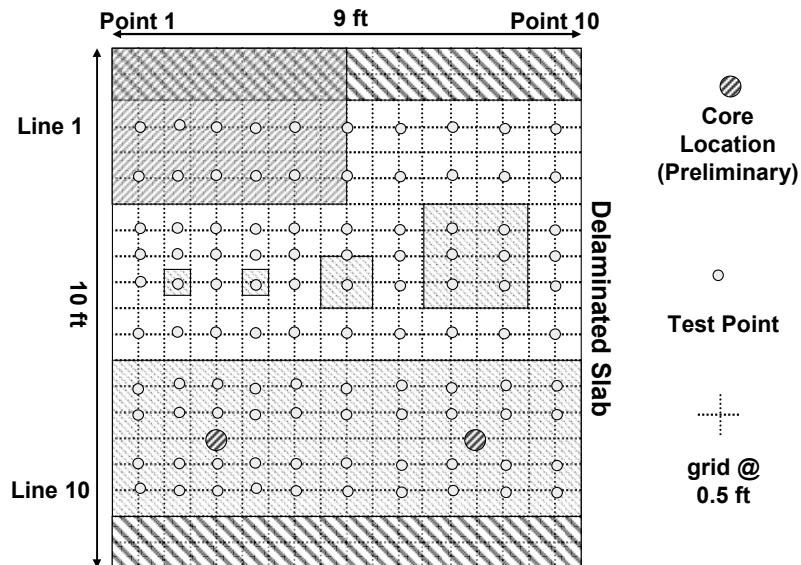

Figure 3. Location of Test Points for Each Section Investigated.

Several debonding agents were used to simulate different levels of debonding. Bond strengths were measured in the laboratory by conducting direct shear tests on prepared specimens (see [4] for details). Clay slurry, talcum powder, grease, and thin paper soaked in motor oil were considered as debonding agents. A tack coat in compliance with Item P-603 of FAA Specifications [10] at a rate of 0.14 g/yd2 was used as the control bonding agent. Highest bond strengths were associated with the tack coat and the lowest with a thin paper soaked in motor oil. Based on the shear strength results, sections constructed with the tack coat were considered as fully-bonded. Sections with the clay slurry, talcum powder and grease were

considered as partially-debonded, and those with oily paper as fully-debonded. A severely debonded area was reproduced in the transition area by placing a piece of thick corrugated cardboard and a thick layer of clay slurry.

Shallow and deep debonding was simulated by placing the debonding agent between the top two lifts (at a depth of 2.5 in.) and bottom two lifts (a depth of 5 in.), respectively. The characteristics of all the sections are fully described in Celaya et al. [11]. In the same report, preliminary evaluation with NDT methods on the constructed section were presented. For the sake of brevity, only typical results of the most feasible methods are provided next.

Ground Penetrating Radar

Typical GPR linescans along a line containing debonded areas and locations of the prepared debonding are shown in Figure 4. GPR detected the severely debonded area and some debonded areas. This is noted as stronger (darker) reflections at the layer interfaces. It was found that GPR may be most suitable when the debonding is in severe stages or moisture is present along the interface of the debonded layers.
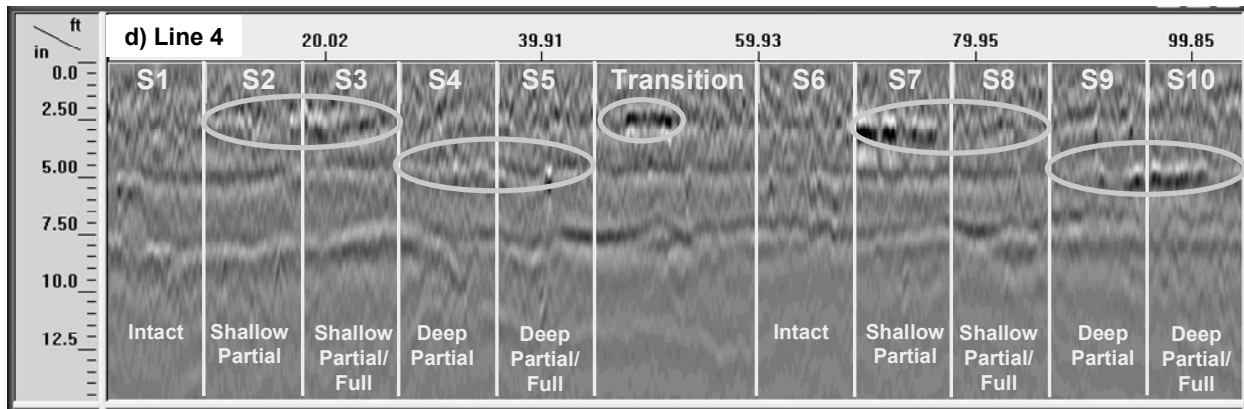

Figure 4. Ground-Coupled GPR Linescans along a Line with Prepared Debonding.

Impulse Response Method

IR test results on a sound and severely debonded area are shown in Figure 5. The voltage amplitude of the geophone for the severe debonded area was around three to four times as large as compared to the intact location and also much wider, while the amplitude of the load remained similar (see Figures 5a and 5c). The ratio between the load cell and geophone amplitudes can be used initially because of its simplicity where smaller ratio corresponds to greater flexibility of the section and therefore debonded locations. A more appropriate analysis consisted of determining the frequency responses using a Fast-Fourier Transform (FFT) algorithm (see Figures 5b and 5d). For the intact location the amplitude presented a dominant frequency of 300 Hz with amplitude of 4.5 and for the severe debonded the frequency was erratic and the maximum amplitude was close to 30. The ratio of the maximum values of the FFT amplitudes (stiffness) was used to compare the results. Based on the studies conducted on the constructed section, the IR method seemed promising for the detection of the fully-debonded areas both shallow and deep and some of the partially-debonded areas.
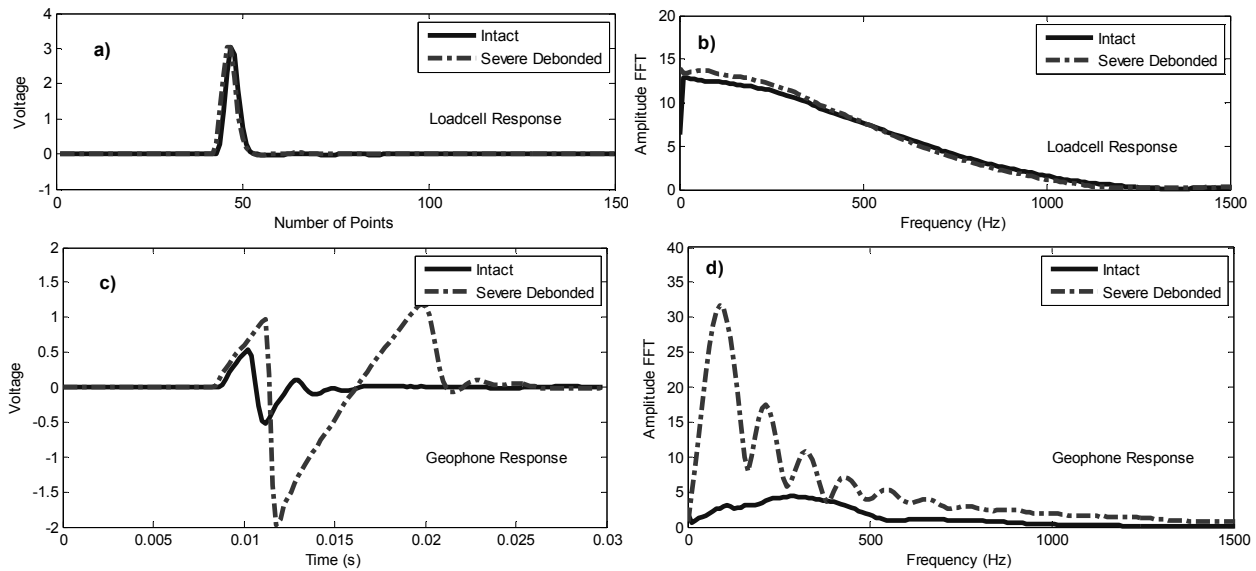
Figure 5. Time Records and FFT Results from IR Examples on Small Scale Study.

Ultrasonic Surface Waves

The PSPA USW analysis pages as seen by the operator in the field are shown in Figure 6 for the intact and severely debonded locations. The graphs demonstrate the variation in modulus with wavelength (called dispersion curves). The dispersion curve for the intact area is fairly uniform; whereas for the damaged point a sharp decrease in modulus below a wavelength of 2.5 in. (63 mm, the location of the damage) is evident. The vertical red lines in the graphs demonstrate the average moduli of the HMA layer from close to surface (1 in., 25 mm) to 8 in. (200 mm, nominal thickness of the layer). As reflected in the left hand side of the two graphs, the average moduli are about 1500 ksi (10 GPa) for the intact and 1130 ksi (7.8 GPa) for the severely-debonded areas. Since HMA modulus is temperature dependent, the values presented were converted to a reference temperature of 77ºF using (Li and Nazarian, [12]). From the controlled section investigation, it was found that the USW method might be able to identify delaminated areas reasonably well, especially the shallow ones.
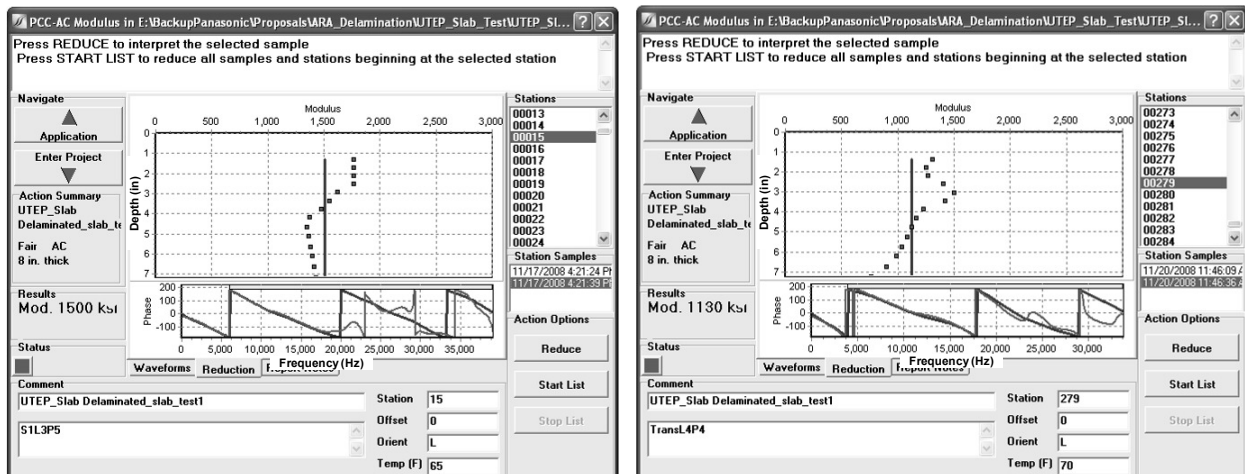
a) Intact   b) Severe Debonding

Figure 6. Dispersion Curve Results with PSPA.

Falling Weight Deflectometer

The FWD used on this study consisted of an impact loading mechanism and a set of seven geophones to measure vertical surface displacements. The first geophone (labeled as SD1) was located right underneath the load plate and each of the other geophones was placed at 1 ft. (300 mm) intervals. Deflections measured for the seven geophones at an intact and the severely debonded locations are shown in Figure 7. Deflections of Geophones 1 and 2 (labeled as SD1 and SD2) are considerably greater at the severe debonded location. For the other five geophones, differences between intact and deboned deflections are small. In general, the FWD did quite well in detecting debonding, although several number of intact locations were identified as inferior. More information and details about the controlled study can be found in Celaya et al., [4].
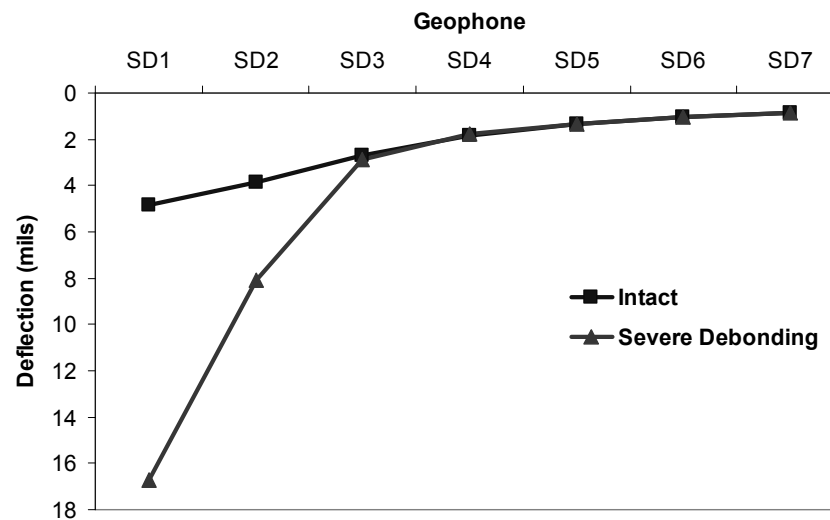

Figure 7. Deflection Examples from FWD on Controlled Study.

FIELD VALIDATION OF NDT TECHNOLOGIES

Even though the evaluation of the methods under controlled condition is valuable, the unanticipated variability in the field conditions and the vastly different operational parameters on actual projects should also be considered. For those reasons, selected NDT methods and test protocols were evaluated on several features of two major international airports in the US: Portland International Airport (PDX) in Oregon and Boston Logan International Airport (BOS) in Massachusetts. It has to be noted that one distinct difference between the airfield features tested and the control section was the substantial differences in the number of layers and thickness of pavement layers tested. Sections at PDX contained severe debonding and stripping problems while BOS mainly contained debonding at about 5 in. depth. PSPA, IR, ground-coupled GPR and FWD (only at PDX because of logistics) were used to estimate the debonded locations. The description of the sites and the results of the NDT evaluation are presented next.

Portland International Airport (PDX) Site

The schematic of PDX and the location of the test sections are shown in Figure 8. Test sections were selected in consultation with PDX staff. Several areas of PDX presented low to medium severity longitudinal cracking. The cracking pattern appeared to indicate that the upper lift of the pavement might be debonded. Several areas of PDX that presented these problems or were suspected of being debonded were selected.
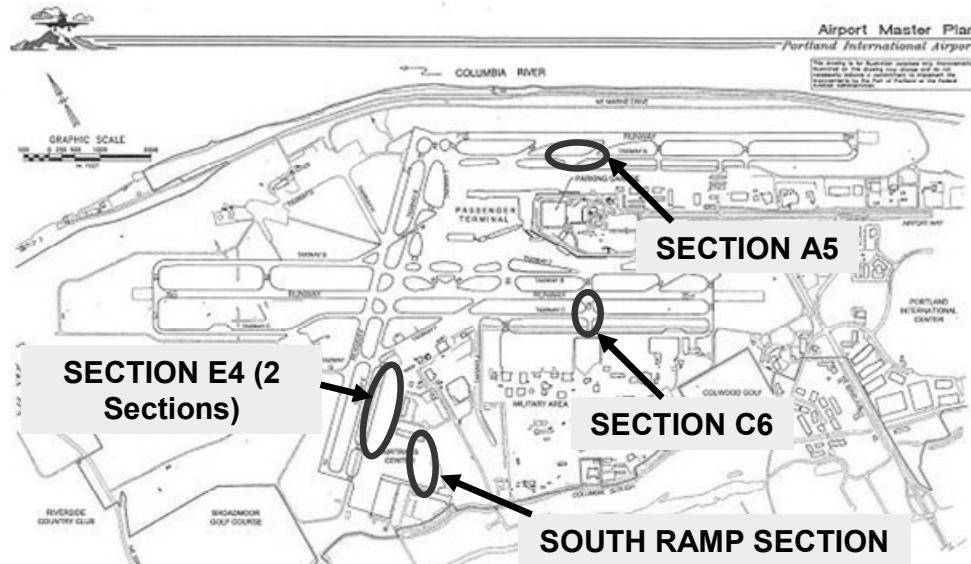
Figure 8. Schematic of PDX and Location of Test Sections.

The suspect areas corresponded to sections of Taxiways A, C and E, and the South Ramp. For the sake of brevity only results obtained on the section investigated on Taxiway A are shown. More information can be found in Celaya et al. [11]. The section investigated on Taxiway A (named A5) was located parallel to Runway 10L/28R near Taxiway A5 (Figure 9). Taxiway A showed longitudinal cracking. Based on cores extracted by PDX staff, cracking was mostly confined to the top asphalt overlay. According to PDX staff, the overlay in some instances was not tightly bonded to the underlying asphalt lifts, and there was some indication of stripping. Ambient temperatures during field tests ranged from 45°F to 70°F.
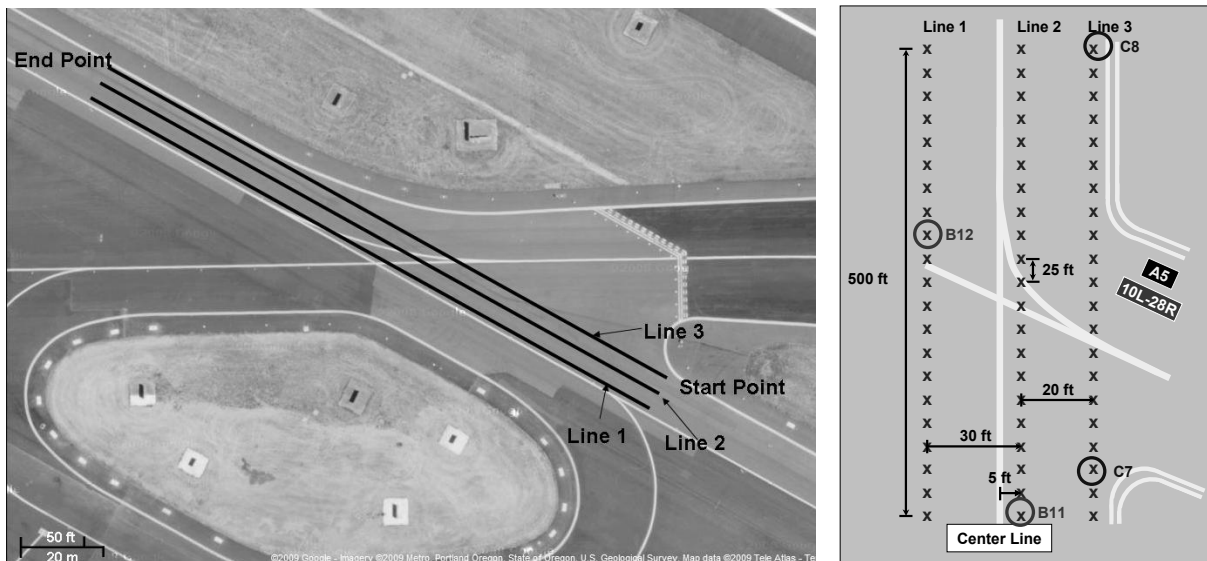
Figure 9. Location of Section A5 and Test Layout.

Ultrasonic surface waves, impulse response, ground-coupled GPR and FWD were used to investigate these sections. Three or four 200- to 500-ft long lines were selected at each site. The GPR tests were carried out along these lines. The other tests were carried out at discrete points between 20 ft. to 50 ft. apart to maximize data coverage. Post-processed GPR linescans along lines 1 and 3 at this section are shown on Figure 10a. Several HMA layer interfaces are
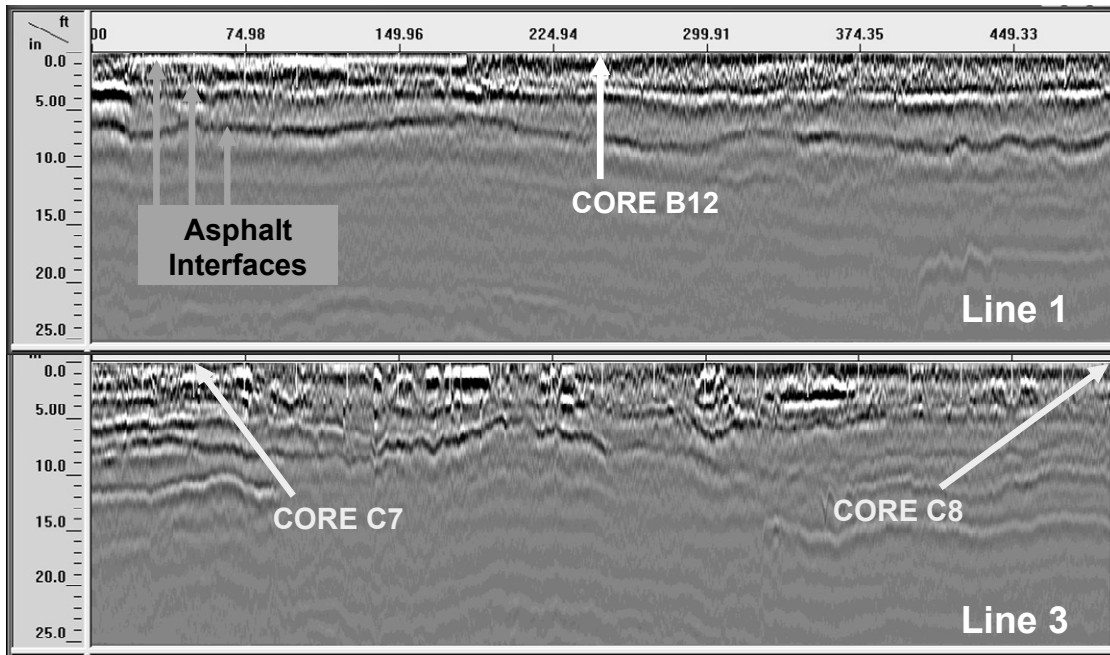
a) GPR Linescans

Distance from Start Point (ft)																				
	0	25	50	75	100	125	150	175	200	225	250	275	300	325	350	375	400	425	450	475	481	500
Line 1	1905	1715	2017	1678	1785	1669	2082	1567	1984	1868	2116	1748	1857	1864	1804	1755	1766	1819	2014	1984	N/A	2026
Line 2	2432	2105	1879	2028	2143	2483	1891	1748	2112	2032	2171	1876	2034	1350	2330	1651	2372	1350	2330	2086	2211	1318
Line 3	1120	1220	1150	1383	1960	1730	1210	1319	1439	1049	1558	1665	1772	1314	1688	1879	1765	2063	1714	1627	N/A	1259

b) PSPA Modulus, E (ksi) $E > E_{avg} - 0.5*\sigma$ $E_{avg} - 0.5*\sigma > E > E_{avg} - \sigma$ $E < E_{avg} - \sigma$

Distance from Start Point (ft)																				
	0	25	50	75	100	125	150	175	200	225	250	275	300	325	350	375	400	425	450	475	481	500
Line 1	6.8	12.3	11.0	10.0	7.6	9.5	10.9	11.1	9.8	6.9	9.1	5.7	9.3	10.7	6.4	6.6	4.6	5.5	5.5	5.5	N/A	6.1
Line 2	9.8	8.7	9.0	11.6	6.7	11.4	12.5	8.1	7.5	7.7	9.0	5.9	11.0	12.1	13.9	6.3	7.7	3.9	6.5	7.4	6.8	8.4
Line 3	2.6	2.0	2.0	2.2	7.4	9.7	8.4	4.1	5.3	6.0	3.5	8.4	6.0	9.9	5.0	4.1	4.2	4.2	3.5	3.4	N/A	4.0

c) IR Results, R (FFT Ratios) $R > R_{avg} - 0.5*\sigma$ $R_{avg} - 0.5*\sigma > R > R_{avg} - \sigma$ $R < R_{avg} - \sigma$

Distance from Start (ft)										
	0	50	100	150	200	250	300	350	400	450	500
Line 1	10.2	9.4	9.5	9.5	8.8	8.9	9.2	9.9	9.6	13.6	14.4
Line 2	11.3	10.3	8.9	8.6	8.7	9.7	8.8	7.2	9.7	13.2	12.7
Line 3	20.9	29.0	9.9	10.4	9.7	8.4	9.5	15.5	16.3	16.1	15.9

d) FWD Deflections (mils) under the load plate (SD1) $SD1 < SD1_{avg} - 0.5*\sigma$ $SD1_{avg} - 0.5*\sigma < SD1 < SD1_{avg} - \sigma$ $SD1 > SD1_{avg} - \sigma$

Figure 10. NDT Results on Section A5.

identified. Some of these interfaces showed stronger reflections that might indicate the presence of trapped moisture or the existence of stripping or debonding, particularly for the first 200 ft. The results from the other NDT methods are also shown in Figures 10b, 10c and 10d. All methods and analyses point to problems along Line 3. Table 1 contains the results of the four confirmatory cores extracted from this section. The results from the three mechanical tests (i.e., PSPA, IR, FWD) are similar for cores B11, B12 and point to intact sections. Even though the mechanical tests for the other two cores indicate damaged cores, the cores were reasonably intact without any indication of debonding. However, the quality of HMA was in question.

Table 1. Comparison of Core Condition with NDT Results on Section A5 of PDX

Core #	Location	GPR	PSPA	IR	FWD	Condition/Comments
B11	Line 2 @0 ft	Intact	Intact	Intact	Intact	Intact
B12	Line 1 @250 ft	Suspect	Intact	Intact	Intact	Intact
C7	Line 3 @0 ft	Suspect	Damaged	Damaged	Damaged	Low quality HMA, Core broken at 9.5 in.
C8	Line 3 @500 ft	Intact	Damaged	Damaged	Damaged	Low quality HMA, Intact

Boston Logan International Airport (BOS) Site

The schematic of BOS and the location of the test sections are shown in Figure 11. A stretch of Runway 9-27 was tested with several NDT methods concurrent with its rehabilitation in July 2009. Previous studies conducted on Runway 9-27 in January 2009 indicated that several areas exhibited debonding of the top lift, and in occasions, areas of extreme stripping. Based on the interaction with BOS airport staff, two sections were selected for field testing. Section 1 was located between Taxiways E and C and Section 2 between Runway 15/33 and Taxiway D as illustrated on Figure 11. However, only results for Section 1 are presented in this paper.

Figure 11. Schematic of BOS and Location of Test Sections.

The test scheme and test layout on Section 1 is shown in Figure 12. Seven 700-ft long lines, one located along the centerline and the others 25, 37.5 and 50 ft. from the centerline on each side, were considered to maximize data coverage. A total of 29 stations, with a spacing of 25 ft., were investigated on each line. The selected NDT methods used in this section were the PSPA, Impulse Response and GPR. Due to operational constraints FWD was not conducted. In addition, five core locations previously retrieved were evaluated with some of the NDT methods. The approximate core locations are also included in Figure 12. From the field inspection it was also observed that some areas of this section exhibited cracking. In addition, the middle 70 ft. of the runaway had been rehabilitated a few years before showing different asphalt characteristics on the surface mat. Ambient temperatures during field tests ranged from 75°F to 100°F.
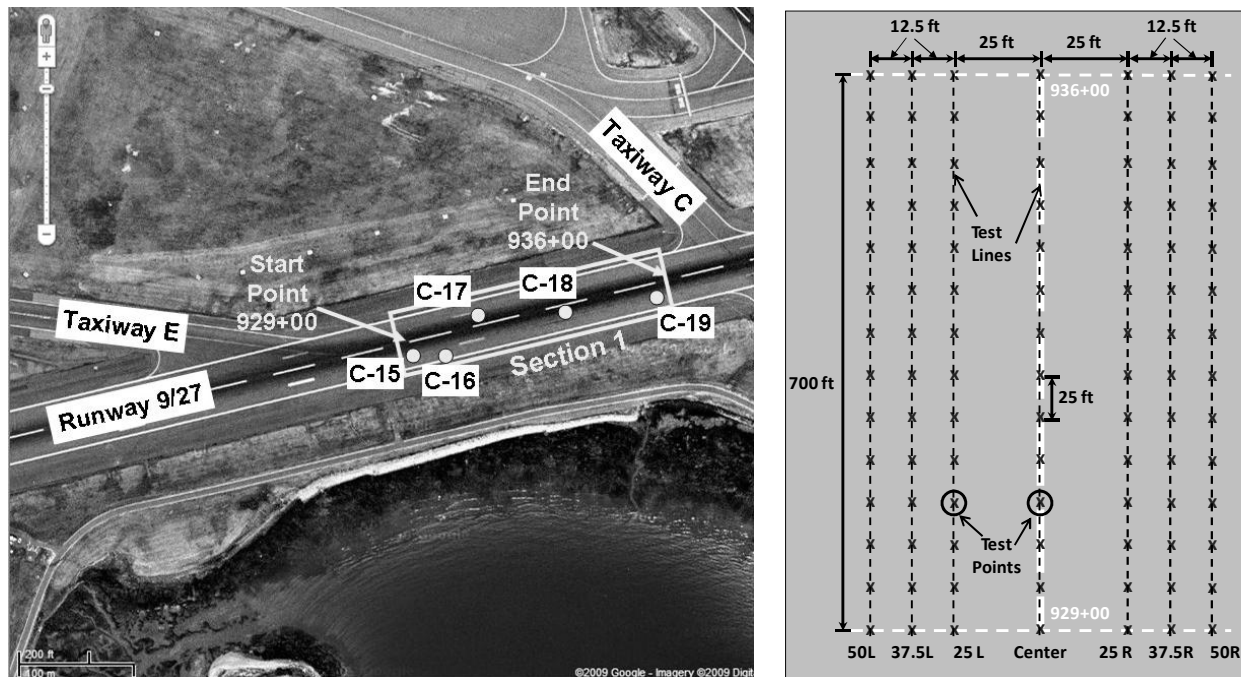

Figure 12. Location of Section 1 and Test Layout.

Post-processed GPR linescans are shown in Figure 13a. Only two of the seven lines are shown for reference (see Celaya et al. [11] for more details). Several horizontal lines associated with the HMA interfaces are marked. Three HMA lifts are observed on all lines at depths of about 2 in., 4 in. and 6 in. Some of these interfaces show strong reflections that might indicate the presence of trapped moisture, stripping or debonding. In addition, some irregularities were identified. The PSPA and IR results are also illustrated in Figure 13 for the seven lines of Section 1. Based on both methods, the worst conditions are observed mostly about the centerline. Most of the points on these lines were identified as marginal or damaged. Dispersion curves from PSPA tests showed stronger reduction in modulus for points about the centerline of the runway.

The conditions of the five cores previously retrieved are compared with the interpretation of the results from NDT devices in Table 2. The conditions of Cores C-15 (intact core) and C-18 (debonded core at 3 in.) as shown in Figure 14 correlated well with the results with the PSPA and IR method. Some discrepancy was found on core C-17 (debonded at 6 in. depth), since PSPA showed marginal condition and IR intact condition, respectively.
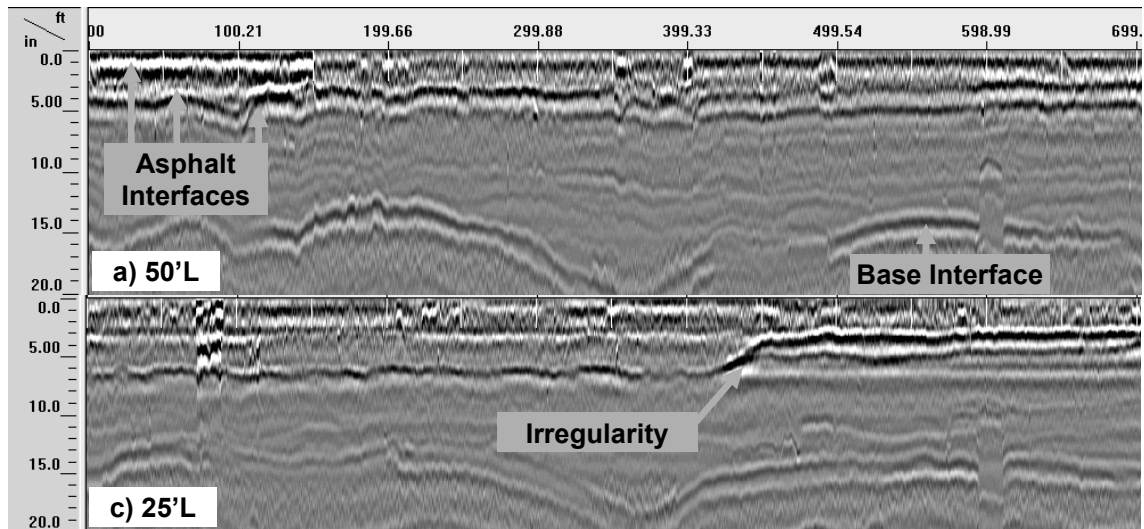
a) GPR Linescans along Section 1

b) PSPA Modulus, E (ksi)

	92900	92925	92950	92975	93000	93025	93050	93075	93100	93125	93150	93175	93200	93225	93250	93275	93300	93325	93350	93375	93400	93425	93450	93475	93500	93525	93550	93575	93600
L50	807	1,021	930	1,072	790	1,798	1,383	1,607	787	1,614	1,384	1,792	1,712	1,873	1,815	1,655	1,059	1,838	1,751	1,664	1,896	1,908	1,942	1,850	816	2,287	2,213	1,941	1,998
L37.5	799	1,188	556	1,082	823	635	1,150	997	1,601	1,110	1,998	897	814	931	601	554	548	2,036	2,129	2,129	1,536	2,187	2,226	1,991	2,109	2,179	2,321	2,036	1,937
L25	963	790	823	1,407	1,007	926	963	1,059	867	1,016	847	921	1,003	839	1,141	891	911	771	832	882	902	659	971	1,219	1,129	1,030	1,080	991	1,055
0	402	780	329	385	642	393	298	436	338	549	597	402	680	613	289	565	683	596	247	887	1,259	974	414	358	277	398	277	256	305
R25	690	975	259	594	549	716	581	489	553	654	737	655	682	1,178	609	573	524	425	488	272	542	359	553	569	554	418	375	368	337
R37.5	1,815	1,334	1,539	1,497	1,456	376	2,423	2,024	1,269	1,018	2,007	1,934	1,726	352	701	1,402	415	1,084	1,564	930	1,634	1,778	1,634	1,426	2,075	1,964	1,557	1,425	1,181
R50	1,464	1,360	1,256	1,194	1,659	1,738	1,615	1,677	1,811	1,331	1,180	1,319	1,319	2,089	1,416	1,978	1,402	2,088	1,130	2,432	1,735	2,235	2,012	2,012	1,554	2,099	1,669	2,124	1,931

$E > E_{avg} - 0.5*\sigma$ $E_{avg} - 0.5*\sigma > E > E_{avg} - \sigma$ $E < E_{avg} - \sigma$

c) IR Results, R (FFT Ratios)

	92900	92925	92950	92975	93000	93025	93050	93075	93100	93125	93150	93175	93200	93225	93250	93275	93300	93325	93350	93375	93400	93425	93450	93475	93500	93525	93550	93575	93600
L50	6.21	3.79	1.96	2.49	2.70	3.65	4.82	5.71	5.68	7.49	7.37	4.58	6.76	4.87	5.77	5.46	7.44	5.42	4.66	6.23	8.38	6.44	4.91	7.20	6.26	5.26	7.50	6.62	4.33
L37.5	4.66	5.15	4.36	3.28	6.04	3.46	6.57	6.80	9.56	9.08	6.10	4.42	3.51	5.21	4.10	3.28	1.97	5.79	5.19	5.70	6.08	6.53	6.24	4.97	5.52	4.50	6.09	6.17	6.89
L25	1.13	2.77	2.89	1.32	1.87	1.75	2.81	1.83	2.20	1.54	2.54	3.24	3.69	4.17	2.84	3.41	3.59	2.76	3.38	3.06	7.14	2.21	4.22	8.27	4.53	6.24	6.75	3.96	4.16
0	0.56	0.91	1.87	1.49	0.96	0.44	0.98	0.61	0.69	0.71	0.59	0.87	0.89	0.20	0.41	0.50	0.84	0.49	0.21	0.47	0.36	0.33	0.37	1.25	0.19	0.40	0.14	0.44	0.42
R25	0.87	0.60	0.71	0.52	0.63	1.03	0.34	1.78	0.55	0.41	1.03	1.57	2.28	1.83	1.01	4.04	0.94	0.36	0.81	0.62	0.60	0.41	1.48	0.74	0.68	0.58	0.42	0.45	1.32
R37.5	5.01	4.36	1.71	1.32	0.72	0.84	2.18	2.26	2.10	3.10	4.72	5.39	1.73	1.46	1.37	2.11	2.64	3.31	2.20	3.94	4.85	4.55	7.54	4.76	4.21	3.85	4.34	6.71	5.48
R50	2.30	3.49	3.17	3.92	0.89	1.93	3.25	6.17	2.48	3.88	2.67	3.44	2.74	5.50	4.26	7.26	2.90	4.80	1.75	4.50	2.51	4.47	4.22	3.92	9.15	2.99	2.65	5.03	6.22

$R > R_{avg} - 0.5*\sigma$ $R_{avg} - 0.5*\sigma > R > R_{avg} - \sigma$ $R < R_{avg} - \sigma$

Figure 13. Post-processed GPR Linescans and other NDT Results on Section 1 of BOS.

Table 2. Comparison of Core Condition with NDT Results on Section 1 of BOS

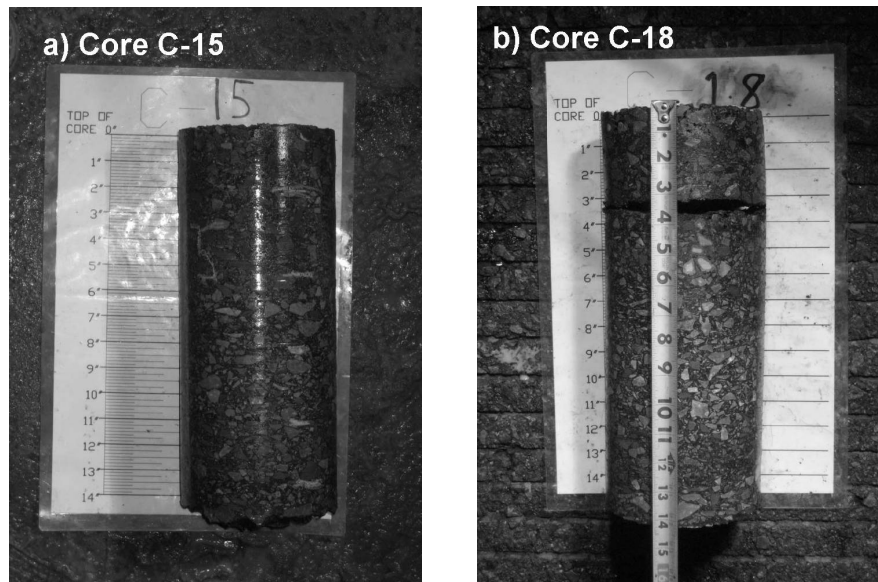| Core #	Location	GPR	PSPA	IR	Condition/Comments
C-15	929+50 @40'R	Intact	Intact	Intact	Intact
C-16	931+00 @60'R	Damaged	N/A	N/A	Intact
C-17	932+50 @10'L	Damaged	Marginal	Intact	Debonding at 6 in.
C-18	934+00 @10'R	Damaged	Damaged	Damaged	Debonding at 3 in.
C-19	935+50 @40'R	Damaged	N/A	N/A	Debonding at 7 in.

Figure 14. Cores Retrieved from Section 1 of BOS.

SUMMARY AND CONCLUSIONS

Several NDT methodologies with potential to detect the debonding of the HMA were extensively evaluated on a control section specifically constructed with various levels of debonding at different depths and with different HMA mixes. From an initial evaluation of about a dozen technologies, the ground-coupled GPR, IR, PSPA and FWD were considered for a comprehensive evaluation as discussed in Celaya et al. [4]. The focus of this paper was to present the evaluation of these four NDT methods at two major US airports. Based on the outcome of the study, the following statements and practical recommendations can be made:

- These two case studies for the most part confirmed the reasonableness of the conclusions drawn from the controlled study. They also revealed some of the complexities of field testing of airport sections.
- In general, all methods were capable to locate damaged areas with a probability of success greater than 50% when compared to ground truth data.
- The higher predictive power at PDX airport can be attributed to the existence of severely debonded and stripped locations that were absent at BOS airport.
- The number of intact points that was not identified as intact is as high as 43%. Even though the cores from these points were not debonded, a majority of them exhibited visible micro-cracking or lower quality HMA with depth.
- It was found that all mechanical NDT methods (PSPA, IR and FWD) detected shallow (less than 3 in. deep) severely debonded areas with reasonable certainty.
- The results from the GPR seemed to be ambiguous.
- For complex pavement sections, the effectiveness of the FWD somewhat diminishes.
- One lesson learned is that the delineation of the low-quality HMA from debonded area is difficult from all mechanical NDT methods. More sophisticated processing of the data should be considered to see whether this problem can be overcome.

ACKNOWLEDGEMENTS

REFERENCES

1. www.usroads.com/journals/rmj/9704/rm970403.htm. Road Management & Engineering Journal. Article Outlines Six Steps to Patching Potholes, April 1, 1997. *Website accessed February 2008.*
2. Bognacki, C. J., Frisvold, A. and Bennert, T. (2007), "Investigation of asphalt pavement slippage failures on Runway 4R-22L, Newark International Airport." FAA Worldwide Airport Technology Transfer Conference. Atlantic City, New Jersey, USA.
3. Hammons, M., I., Von Quintus, H., Maser, K., and Nazarian, S. (2005) "Detection of stripping in hot mix asphalt." Applied Research Associates Project Number 16355, prepared for: Office of Materials and Research, Georgia Department of Transportation.
4. Celaya, M., Mejia, D., Ertem, S., Nazarian, S., Rao, C., Von Quintus, H. and Shokouhi, P. "Evaluation of NDT Technologies to Assess Presence and Extent of Delamination of HMA Airfield Pavements: Verification Study." AAPTP Report for Project 06-04, October 2009.
5. Celaya, M., Nazarian, S., Rao, C., and Von Quintus, H. "Delamination Detection of Asphalt Pavements with Nondestructive Testing Devices." 90th Annual Transportation Research Board Meeting, Washington, DC, 2011.
6. Maser K. R. (1996), "Condition assessment of transportation infrastructure using ground penetrating radar", ASCE Journal of Infrastructure Systems, pp. 94-101.
7. Heitzman, M., Maser, K., Tran, N. H., Brown, R., Bell, H., Holland, S. Ceylan, H., Belli, K., and Hiltunen, D. "Nondestructive Testing to Identify Delaminations Between HMA Layers." SHRP 2 Report S2-R06D-RR-1, Transportation Research Board, Washington, DC, 20113.
8. Kruntcheva, M., R., Collop, A., C. and Thom, N., H. (2004) "Feasibility of assessing bond condition of asphalt concrete layers with dynamic nondestructive testing." Journal of Transportation Engineering, Vol. 130, No. 4.
9. Nazarian, S., Yuan, D., Smith, K., Ansari, F., Gonzalez, C., "Acceptance Criteria of Airfield Concrete Pavement Using Seismic and Maturity Concepts. "Innovative Pavement Research Foundation, Airport Concrete Pavement Technology Program. Report IPRF-01-G-002-02-2, May 2006.
10. Standards for Specifying Construction of Airports. Advisory Circular 150/5370-10E. U.S. Department of Transportation Federal Aviation Administration, 2009.
11. Celaya, M., Mejia, D., Ertem, S., Nazarian, S., Rao, C., Von Quintus, H. and Shokouhi, P. "Evaluation of NDT Technologies to Assess Presence and Extent of Delamination of HMA Airfield Pavements." Airfield Asphalt Pavement Technology Program, Federal Aviation Administration. AAPTP Research Project 06-04, March 2010.
12. Li, Y., and Nazarian, S. (1994), "Evaluation of Aging of Hot-Mix Asphalt Using Wave Propagation Techniques," Engineering Properties of Asphalt Mixtures And the Relationship to Their Performance, ASTM STP 1265, Philadelphia, Pa., pp.166-179.